The Effect of Population Flow on Epidemic Spread: Analysis and Control

Brooks Butler, Ciyuan Zhang, Ian Walter, Nishant Nair, Raphael Stern, and Philip E. Paré*

Abstract

In this paper, we present a discrete-time networked SEIR model using population flow, its derivation, and assumptions under which this model is well defined. We identify properties of the system's equilibria, namely the healthy states. We show that the set of healthy states is asymptotically stable, and that the value of the equilibria becomes equal across all sub-populations as a result of the network flow model. Furthermore, we explore closed-loop feedback control of the system by limiting flow between sub-populations as a function of the current infected states. These results are illustrated via simulation based on flight traffic between major airports in the United States. We find that a flow restriction strategy combined with a vaccine roll-out significantly reduces the total number of infections over the course of an epidemic, given that the initial flow restriction response is not delayed.

I. Introduction

Global interconnectivity has proven to be a key factor in the propagation of infectious diseases [1], [2]. Most recently, we have seen evidence of such connectivity through the rapid spread of the COVID-19 pandemic, which propagated from its origin in Wuhan, China to every major population center globally in a matter of weeks [3]. Given the implications of global population flow on disease spread, it becomes important to accurately model this flow, as reliable modeling is an essential step to developing effective and efficient mitigation strategies. Various infection models have been proposed based on characteristics of individual pathogens and studied in the literature, including susceptible-infected-susceptible (SIS), susceptible-infected-removed (SIR), and susceptible-infected-removed-susceptible (SIRS) [4], [5]. For this paper, we consider the recent COVID-19 pandemic as a motivating case for the model selection and construction. Due to the delay in onset of COVID-19 symptoms [6]–[9] and large asymptomatic populations estimated between $17 - 81\%$ [10]–[13], we choose the susceptible-exposed-infected-removed (SEIR) model as the foundation of our model development.

Previous work involving the incorporation of population flows in epidemic process models include analysis of a networked SIS model with flows [14] as well as using a networked SIR model with flows to predict arrival times for various epidemics using global flight data [15], where both models are developed in continuous time. This paper uses similar derivation techniques to define our discrete-time epidemic model. However, we contribute to the development of such models by including the exposed state in our model formulation, as well as provide analysis of the discrete time dynamics. While other work has considered capturing the effect of transportation on the spread of COVID-19 using the SEIR model [16], the key distinction in this work is that infection propagation over the network is modeled by the relocation of infected individuals

to other sub-populations rather than assuming direct contact and intermingling between sub-populations. Furthermore, while previous work assumes the likelihood of individuals traveling is independent of their infection state, this work considers the effect of being infected on the probability of an individual traveling.

A. Contributions

In this paper, we explore a discrete-time networked SEIR model to analyze the effect of population flows on the propagation of an infectious disease. We summarize the contributions of this paper as follows:

1) We derive a discrete-time networked SEIR model incorporating population flows, including the conditional probabilities of a given state affecting the likelihood of an individual to be traveling.
2) We present assumptions on the parameters for the model to be well defined given proper initial conditions.
3) We prove model convergence and show that the equilibria (i.e., the healthy states) are homogeneous, that is, the same value for all sub-populations.
4) We present a feedback control law that restricts system flow globally using the infection states, show that under the control effort the model is still well defined, and illustrate its behavior via simulation.

In the remainder of this paper, we present our model derivation and necessary assumptions in Section II, provide analysis of the healthy states in Section III, propose a feedback control in Section IV, and illustrate the model and the effectiveness of the controller through simulation in Section V. Finally, we provide our conclusions in Section VI.

B. Notation

We denote the set of real numbers, positive real numbers, non-negative integers, and the positive integers as $\mathbb{R}$, $\mathbb{R}_{>0}$, $\mathbb{Z}_{\geq 0}$, and $\mathbb{Z}_{\geq 1}$, respectively. For any positive integer n, we have $[n] = \{1, 2, ..., n\}$. A diagonal matrix is denoted as $\text{diag}(\cdot)$. The transpose of a vector $x \in \mathbb{R}^n$ is $x^\top$. We use $\mathbf{0}$ and $\mathbf{1}$ to denote the vectors whose entries all equal 0 and 1, respectively. We let $\mathcal{G} = (\mathbb{V}, \mathbb{E}, \mathbb{W})$ denote a weighted directed graph where $\mathbb{V} = \{v_1, v_2, ..., v_n\}$ is the set of nodes, $\mathbb{E} \subseteq \mathbb{V} \times \mathbb{V}$ is the set of edges, and $\mathbb{W} : \mathbb{E} \to \mathbb{R}_{>0}$ maps to the real valued edge weights on each edge. We denote the configuration of edges in a directed graph at time step k as $\mathcal{G}^k = (\mathbb{V}, \mathbb{E}^k, \mathbb{W})$, where $\mathbb{E}^k$ denotes the set of edges at time step k. Furthermore, we denote $\cup_{k \geq 0} \mathbb{E}^k$ as the union of all non-zero edge configurations on a graph for all $k \geq 0$. We define a graph $\mathcal{G}$ as being strongly connected if there is a path from every node to every other node in the graph.

II. SEIR MODEL WITH NETWORK FLOWS

In this section, we present a networked SEIR model incorporating the population flow of individuals between sub-populations. First, consider a group of n sub-populations in a graph, where each sub-population $i \in [n]$ is represented by a node in the graph. We use the SEIR model to describe how suceptible individuals in sub-population i become exposed, infected, and eventually recover as the result of an infectious disease [17]. We begin with defining the SEIR model behavior without graph connections for each sub-population $i \in [n]$ where S_i, E_i, I_i, and R_i represent the number of susceptible,

exposed, infected, and recovered individuals in sub-population i, respectively,

$$\dot{S}_i(t) = -\beta_i(t)\frac{I_i(t)}{N_i}S_i(t) \tag{1a}$$

$$\dot{E}_i(t) = \beta_i(t)\frac{I_i(t)}{N_i}S_i(t) - \sigma_i(t)E_i(t) \tag{1b}$$

$$\dot{I}_i(t) = \sigma_i(t)E_i(t) - \delta_i(t)I_i(t) \tag{1c}$$

$$\dot{R}_i(t) = \delta_i(t)I_i(t), \tag{1d}$$

where β_i is the infection rate, σ_i is transition rate from exposed to infected, and δ_i is the healing rate. We assume $S_i(t) + E_i(t) + I_i(t) + R_i(t) = N_i$ for all t, i.e., a fixed population size for each sub-population. We assume fixed sub-populations as the intended time scale of the model is such that population change due to birth/death rates and migration is negligible (e.g. rapid disease propagation over weeks or months). While all the variables (and model parameters, except population), will (may) continue to vary with time, we remove the time-dependence notation for convenience and ease of reading from this point forward.

To account for the flow of individuals between sub-populations we we expand the model in (1):

$$\dot{S}_i = -\beta_i\frac{I_i}{N_i}S_i + \sum_{j\neq i}\left(F_{ij}\frac{S_j}{N_j} - F_{ji}\frac{S_i}{N_i}\right) \tag{2a}$$

$$\dot{E}_i = \beta_i\frac{I_i}{N_i}S_i - \sigma_iE_i + \sum_{j\neq i}\left(F_{ij}\frac{E_j}{N_j} - F_{ji}\frac{E_i}{N_i}\right) \tag{2b}$$

$$\dot{I}_i = \sigma_iE_i - \delta_iI_i + \sum_{j\neq i}\left(F_{ij}\frac{I_j}{N_j} - F_{ji}\frac{I_i}{N_i}\right) \tag{2c}$$

$$\dot{R}_i = \delta_iI_i + \sum_{j\neq i}\left(F_{ij}\frac{R_j}{N_j} - F_{ji}\frac{R_i}{N_i}\right), \tag{2d}$$

where F_{ij} represents the number of individuals flowing from sub-population j to i, where $F_{ii} = 0$. By making a substitution of variables where $s_i = S_i/N_i, e_i = E_i/N_i, x_i = I_i/N_i, r_i = R_i/N_i$ we can model the proportion of individuals as follows

$$\dot{s}_i = -\beta_ix_is_i + \frac{1}{N_i}\sum_{j\neq i}(F_{ij}s_j - F_{ji}s_i) \tag{3a}$$

$$\dot{e}_i = \beta_ix_is_i - \sigma_ie_i + \frac{1}{N_i}\sum_{j\neq i}(F_{ij}e_j - F_{ji}e_i) \tag{3b}$$

$$\dot{x}_i = \sigma_ie_i - \delta_ix_i + \frac{1}{N_i}\sum_{j\neq i}(F_{ij}x_j - F_{ji}x_i) \tag{3c}$$

$$\dot{r}_i = \delta_ix_i + \frac{1}{N_i}\sum_{j\neq i}(F_{ij}r_j - F_{ji}r_i), \tag{3d}$$

where $s_i + e_i + x_i + r_i = 1$. Note that both (2) and (3) assume the sub-populations are well mixed and that the likelihood of an individual traveling is independent of their infectious state, that is, whether they are susceptible, exposed, infected, or

recovered. We now extend our model to include the probability that an individual is traveling, given their infectious state.

$$\dot{s}_i = -\beta_i x_i s_i + \frac{1}{N_i} \sum_{j \neq i} (F_{ij} P(s_j|T_j) - F_{ji} P(s_i|T_i)) \tag{4a}$$

$$\dot{e}_i = \beta_i x_i s_i - \sigma_i e_i + \frac{1}{N_i} \sum_{j \neq i} (F_{ij} P(e_j|T_j) - F_{ji} P(e_i|T_i)) \tag{4b}$$

$$\dot{x}_i = \sigma_i e_i - \delta_i x_i + \frac{1}{N_i} \sum_{j \neq i} (F_{ij} P(x_j|T_j) - F_{ji} P(x_i|T_i)) \tag{4c}$$

$$\dot{r}_i = \delta_i x_i + \frac{1}{N_i} \sum_{j \neq i} (F_{ij} P(r_j|T_j) - F_{ji} P(r_i|T_i)), \tag{4d}$$

where $P(q_i|T_i)$, $q_i \in \{s_i, e_i, x_i, r_i\}$ is the probability of an individual at sub-population i being in a certain infectious state given that they are also traveling. Note that

$$P(s_i|T_i) + P(e_i|T_i) + P(x_i|T_i) + P(r_i|T_i) = 1 \tag{5}$$

for all $i \in [n]$. We can compute the probability that an individual from sub-population i is traveling given that they are in state q_i using Bayes' rule,

$$P(q_i|T_i) = \frac{P(T_i|q_i)P(q_i)}{P(T_i)}, \tag{6}$$

where $P(T_i)$ is the probability of an individual traveling from sub-population i and $P(q_i) = q_i$ is the probability they are in state q_i. We compute the probability of an individual traveling from a given sub-population $i \in [n]$ as

$$P(T_i) = \gamma_i = \frac{\sum_{j \neq i} F_{ji}}{N_i}, \tag{7}$$

where γ_i is the proportion of the population flowing out of sub-population i and $\gamma_i \in [0, 1]$ as it is reasonable to assume that $\sum_{j \neq i} F_{ji} \ll N_i$ (as $\sum_{j \neq i} F_{ji} = N_i$ would imply that the entire population is traveling at a given time). Since measuring $P(q_i|T_i)$ is practically challenging, we instead parameterize $p_i^q := P(T_i|q_i)$, for $q_i \in \{s_i, e_i, x_i, r_i\}$, as follows. Using (5)-(7) we have that

$$\frac{1}{\gamma_i}(p_i^s s_i + p_i^e e_i + p_i^x x_i + p_i^r r_i) = 1. \tag{8}$$

Therefore, assuming that $p_i^s = p_i^e = p_i^r = p_i^T$, we have

$$p_i^T(s_i + e_i + r_i) + p_i^x x_i = \gamma_i.$$

Thus, solving for p_i^T yields

$$p_i^T = \frac{\gamma_i - p_i^x x_i}{s_i + e_i + r_i}, \tag{9}$$

which allows us to use $p_i^x \in [0, 1]$ as a parameter to describe how likely an individual will be traveling given that they are infected. Furthermore, we can compute the number of individuals flowing from sub-population j to i as

$$F_{ij} = \gamma_j w_{ij} N_j, \tag{10}$$

where w_{ij} is the proportion of traveling individuals flowing from sub-population j to i computed as

$$w_{ij} = \frac{F_{ij}}{\sum_{l \neq j} F_{lj}} \tag{11}$$

with $w_{ii} = 0$. Thus, we can derive the dynamics for the susceptible proportion at sub-population i as

$$\dot{s}_i = -\beta_i x_i s_i + \frac{1}{N_i} \sum_{j \neq i} (F_{ij} P(s_j | T_j) - F_{ji} P(s_i | T_i))$$

$$= -\beta_i x_i s_i + \frac{1}{N_i} \sum_{j \neq i} \left(\gamma_j w_{ij} N_j \frac{p_j^T s_j}{\gamma_j} - \gamma_i w_{ji} N_i \frac{p_i^T s_i}{\gamma_i} \right)$$

$$= -\beta_i x_i s_i + \sum_{j \neq i} \left(\frac{N_j}{N_i} w_{ij} p_j^T s_j - w_{ji} p_i^T s_i \right).$$

Using the fact that $\sum_{j \neq i} w_{ji} = 1$, by (11), we have that

$$\dot{s}_i = -(\beta_i x_i + p_i^T) s_i + \sum_{j \neq i} \frac{N_j}{N_i} w_{ij} p_j^T s_j.$$

By similar derivations, we can rewrite (4) as

$$\dot{s}_i = -(\beta_i x_i + p_i^T) s_i + \sum_{j \neq i} \frac{N_j}{N_i} w_{ij} p_j^T s_j \tag{12a}$$

$$\dot{e}_i = \beta_i x_i s_i - (\sigma_i + p_i^T) e_i + \sum_{j \neq i} \frac{N_j}{N_i} w_{ij} p_j^T e_j \tag{12b}$$

$$\dot{x}_i = \sigma_i e_i - (\delta_i + p_i^x) x_i + \sum_{j \neq i} \frac{N_j}{N_i} w_{ij} p_j^x x_j \tag{12c}$$

$$\dot{r}_i = \delta_i x_i - p_i^T r_i + \sum_{j \neq i} \frac{N_j}{N_i} w_{ij} p_j^T r_j. \tag{12d}$$

We choose to discretize our model due to the nature of the collected data on the spread of pandemics, where the highest resolution data is typically recorded once per day. Using Euler's method, we can write (12) in discrete time as

$$s_i^{k+1} = s_i^k + h \left(-(\beta_i^k x_i^k + p_i^{T,k}) s_i^k + \sum_{j \neq i} \frac{N_j}{N_i} w_{ij}^k p_j^{T,k} s_j^k \right) \tag{13a}$$

$$e_i^{k+1} = e_i^k + h \left(\beta_i^k x_i^k s_i^k - (\sigma_i^k + p_i^{T,k}) e_i^k + \sum_{j \neq i} \frac{N_j}{N_i} w_{ij}^k p_j^{T,k} e_j^k \right) \tag{13b}$$

$$x_i^{k+1} = x_i^k + h \left(\sigma_i^k e_i^k - (\delta_i^k + p_i^{x,k}) x_i^k + \sum_{j \neq i} \frac{N_j}{N_i} w_{ij}^k p_j^{x,k} x_j^k \right) \tag{13c}$$

$$r_i^{k+1} = r_i^k + h \left(\delta_i^k x_i^k - p_i^{T,k} r_i^k + \sum_{j \neq i} \frac{N_j}{N_i} w_{ij}^k p_j^{T,k} r_j^k \right), \tag{13d}$$

where $k \in \mathbb{Z}_{\geq 0}$ is a given time step and $h \in \mathbb{R}_{>0}$ is a sampling parameter, yielding our discrete time model.

For the model in (13) to be well-defined we require the following assumptions.

Assumption 1. *Let $\sum_{i \neq j} F_{ij}^k = \sum_{i \neq j} F_{ji}^k$ for all $i \in [n]$ and $k \in \mathbb{Z}_{\geq 0}$.*

This assumption requires that the total flow of individuals into a given sub-population must be equal to the total flow out. Furthermore, we impose the following assumption on the model parameters.

Assumption 2. *For all $i \in [n]$ and $k \in \mathbb{Z}_{\geq 0}$, let $\beta_i^k, \delta_i^k, \sigma_i^k \in \mathbb{R}_{>0}$, $h\beta_i^k, h\delta_i^k, h\sigma_i^k \in (0, 1]$, $h(\beta_i^k + p_i^{T,k}) \leq 1$, $h(\sigma_i^k + p_i^{T,k}) \leq 1$, and $h(\delta_i^k + p_i^{T,k}) \leq 1$.*

Under these assumptions, we can show that given proper initial conditions the model will always remain well defined.

Lemma 1. *Consider the model in* (13) *under Assumptions 1-2. Suppose* $s_i^0, e_i^0, x_i^0, r_i^0 \in [0,1]$ *and* $s_i^0 + e_i^0 + x_i^0 + r_i^0 = 1$ *for all* $i \in [n]$. *Then, for all* $k \geq 0$ *and* $i \in [n]$, $s_i^k, e_i^k, x_i^k, r_i^k \in [0,1]$ *and* $s_i^k + e_i^k + x_i^k + r_i^k = 1$.

Proof. We prove the result by induction. By assumption, it holds for the base case $k = 0$. We now show the inductive step, where given $s_i^k, e_i^k, x_i^k, r_i^k \in [0,1]$ and $s_i^k + e_i^k + x_i^k + r_i^k = 1$ for all $i \in [n]$, we show that the same holds for $k + 1$. By (13) and Assumption 2 we have

$$q_i^{k+1} \geq h \sum_{j \neq i} \frac{N_j}{N_i} w_{ij}^k p_j^{T,k} q_j^k \geq 0, \tag{14}$$

where $q_i^k \in \{s_i^k, e_i^k, x_i^k, r_i^k\}$ for all $i \in [n]$ and $k \in \mathbb{Z}_{\geq 0}$.

Furthermore, computing $s_i^{k+1} + e_i^{k+1} + x_i^{k+1} + r_i^{k+1}$ yields

$$
\begin{aligned}
s_i^{k+1} + e_i^{k+1} + x_i^{k+1} + r_i^{k+1} &= s_i^k + e_i^k + x_i^k + r_i^k + h\left(-\beta_i^k x_i^k s_i + \beta_i^k x_i^k s_i - \sigma_i^k e_i^k + \sigma_i^k e_i^k - \delta_i^k x_i^k + \delta_i^k x_i^k\right) \\
&\quad + \frac{h}{N_i} \sum_{j \neq i} \left(F_{ij}^k (P(s_i|T_i) + P(e_i|T_i) + P(x_i|T_i) + P(r_i|T_i)) - F_{ji}^k (P(s_j|T_j) + P(e_j|T_j) + P(x_j|T_j) + P(r_j|T_j))\right) \\
&= s_i^k + e_i^k + x_i^k + r_i^k + \frac{h}{N_i}\left(F^+ - F^-\right) = 1, \tag{15}
\end{aligned}
$$

where $F^+ = \sum_{j \neq i} F_{ij}^k$ and $F^- = \sum_{j \neq i} F_{ji}^k$ denote the total flow in and out of each sub-population, respectively, which are equal by Assumption 1. Since each variable is non-negative by (14) and their sum must add to one by (15), we have that $s_i^{k+1}, e_i^{k+1}, x_i^{k+1}, r_i^{k+1} \leq 1$. Thus, we have shown that $s_i^{k+1}, e_i^{k+1}, x_i^{k+1}, r_i^{k+1} \in [0,1]$, completing the inductive step. □

Remark 1. *Assumption 2 requires that the sampling parameter be small enough in relation to the model spread parameters such that the model remains well defined. Furthermore, requiring* $h(\beta_i^k x_i^k + p_i^{T,k}) \leq 1, h(\sigma_i^k + p_i^{T,k}) \leq 1$, *and* $h(\delta_i^k + p_i^{T,k}) \leq 1$ *can be interpreted as requiring that no individual can both travel and transition between infectious states during the same time step* $k \in \mathbb{Z}_{\geq 0}$, *as our model does not capture infection occurring during travel.*

The following are not required for the model to remain well defined. However, we use them in the next section to show that the set of healthy states have a homogeneous structure.

Definition 1. *A graph* $\mathcal{G}^k = (\mathbb{V}, \cup_{k \geq 0} \mathbb{E}^k, \mathbb{W})$ *for* $k \in \mathbb{Z}_{\geq 0}$ *is* <u>K-strongly connected</u> *if there exist some bound* K *such that* $(\mathbb{V}, \cup_{j=k}^{k+K-1} \mathbb{E}^j, \mathbb{W})$ *is strongly connected, for all* $k \in \mathbb{Z}_{\geq 0}$.

Assumption 3. *Let the graph* $\mathcal{G}^k = (\mathbb{V}, \cup_{k \geq 0} \mathbb{E}^k, \mathbb{W})$, *where* $\mathbb{W} : \mathbb{E}^k \to \mathbb{R}_{>0}$ *is defined by* w_{ij}^k, *be K-strongly connected.*

III. MODEL ANALYSIS

In this section we analyze the equilibria of the model in (13), i.e., the healthy states of the system, which we define as $q_i^* = \lim_{k \to \infty} q_i^k$ for all $i \in [n]$ where $q_i^* \in \{s_i^*, e_i^*, x_i^*, r_i^*\}$. We use the following result given in [18] on the conditions for discrete-time consensus models.

Lemma 2. *Let a discrete-time system defined by the transition matrix* L^k *satisfy the following properties, where* l_{ij}^k *is the corresponding entry in the ith row and jth column at time step* $k \in \mathbb{Z}_{\geq 0}$:

(i) The graph $G = (\mathbb{V}, \cup_{k \geq 0} \mathbb{E}^k)$, *where the edge weights at time step k are given by* L^k, *is K-strongly connected.*

(ii) There exists a positive constant $y \in \mathbb{R}_{>0}$ such that for all $i, j \in [n]$ and $k \in \mathbb{Z}_{\geq 0}$ we have

    (a) $l_{ii}^k \geq y$

    (b) $l_{ij}^k \in \{0\} \cup [y, 1]$

    (c) $\sum_{j=1}^n l_{ij}^k = 1$.

Then, the system dynamics defined by L^k guarantee asymptotic consensus.

We now present results on the asymptotic convergence of the healthy states for the system in (13).

Theorem 1. *Consider the model in* (13) *under Assumptions 1-3. Given that there exists some $i \in [n]$ such that $x_i^0 \in (0, 1]$ or $e_i^0 \in (0, 1]$, then there exists a set of asymptotically stable equilibria of the form $(\mathbf{s}^*, \mathbf{0}, \mathbf{0}, 1 - \mathbf{s}^*)$, where $\mathbf{s}^* = \alpha \mathbf{1}$, $\alpha \in [0, 1]$.*

Proof. We prove the result by splitting it into two parts, namely,

1) $e_i^* = 0$ and $x_i^* = 0$, for all $i \in [n]$

2) $s_i^* = \alpha$ for all $i \in [n]$.

The parts are presented sequentially:

1) We denote $\mathbf{S}^k = \sum_{i=1}^n s_i^k \in [0, n]$, $\mathbf{E}^k = \sum_{i=1}^n e_i^k \in [0, n]$ and $\mathbf{X}^k = \sum_{i=1}^n x_i^k \in [0, n]$ as the sum of the susceptible, exposed, and infected states of all the sub-populations, respectively. Hence, based on the dynamics of the system states in (13) and by Assumption 1, we have

$$\mathbf{S}^{k+1} = \mathbf{S}^k - h \sum_{i=1}^n \beta_i^k x_i^k s_i^k \tag{16a}$$

$$\mathbf{E}^{k+1} = \mathbf{E}^k + h \left(\sum_{i=1}^n \beta_i^k x_i^k s_i^k - \sum_{i=1}^n \sigma_i^k e_i^k \right) \tag{16b}$$

$$\mathbf{X}^{k+1} = \mathbf{X}^k + h \left(\sum_{i=1}^n \sigma_i^k e_i^k - \sum_{i=1}^n \delta_i^k x_i^k \right). \tag{16c}$$

By Assumption 2 and Lemma 1, we have that the rate of change of $\mathbf{S}^k$, $-h \sum_{i=1}^n \beta_i^k x_i^k s_i^k$, is non-positive for all $k \geq 0$ and $\mathbf{S}^k$ is lower bounded by zero. Hence, by Lemma 1, we obtain that $\lim_{k \to \infty} \mathbf{S}^k$ exists, and

$$\lim_{k \to \infty} -h \sum_{i=1}^n \beta_i^k x_i^k s_i^k = 0. \tag{17}$$

Accordingly, we can write that $\lim_{k \to \infty} (\mathbf{E}^{k+1} - \mathbf{E}^k) = \lim_{k \to \infty} -h \sum_{i=1}^n \sigma_i^k e_i^k$. From Assumption 2, we know that $h\sigma_i^k > 0$ for all $i \in [n]$ and $k \in \mathbb{Z}_{\geq 0}$. Therefore, by Lemma 1, we conclude that $\lim_{k \to \infty} \mathbf{E}^k = 0$ and thus $\lim_{k \to \infty} e_i^k = 0$ for all $i \in [n]$.

Similarly, we acquire that $\lim_{k \to \infty} (\mathbf{X}^{k+1} - \mathbf{X}^k) = \lim_{k \to \infty} -h \sum_{i=1}^n \delta_i^k x_i^k$, since $\lim_{k \to \infty} e_i^k = 0$ for all $i \in [n]$. By Assumption 2 and Lemma 1, $h\delta_i^k > 0$ and x_i^k is well-defined, we acquire that $\lim_{k \to \infty} \mathbf{X}^k = 0$ and thus $\lim_{k \to \infty} x_i^k = 0$ for all $i \in [n]$.

2) In order to show that the susceptible states become equally mixed as $k \to \infty$, where $k \in \mathbb{Z}_{\geq 0}$, we leverage Lemma 2. First, we construct dynamics for the susceptible states in (13a) when $x_i^* = e_i^* = 0$ for all $i \in [n]$, as proven in 1), which yields

$$s_i^{k+1} = s_i^k + h \left(-\gamma_i^k s_i^k + \sum_{j \neq i} \frac{N_j}{N_i} w_{ij}^k \gamma_i^k s_j^k \right), \tag{18}$$

where $p_i^{T,k} = \gamma_i$ by (9) and Lemma 1. We can express these dynamics in matrix form as

$$s^{k+1} = \underbrace{\left(I + h\left(-\Gamma^k + N^{-1}W^k\Gamma^k N\right)\right)}_{L^k} s^k, \tag{19}$$

where $s^k = [s_1^k, \ldots, s_n^k]^\top$, $\Gamma^k = \text{diag}(\gamma_1^k, \ldots, \gamma_n^k)$, $N = \text{diag}(N_1, \ldots, N_n)$, and W^k is the matrix defined by entries w_{ij}^k on the ith row and jth column. In order to guarantee that s_i^* is homogeneous for all $i \in [n]$, we will apply Lemma 2 to (19).

Property *(i)* of Lemma 2 holds by Assumption 3. Furthermore, *(ii.a)* and *(ii.b)* are true by construction. We now show *(ii.c)* is true by computing $L^k \mathbf{1}$, which yields

$$L^k \mathbf{1} = \mathbf{1} + h\left(-\boldsymbol{\gamma}^k + N^{-1}W^k\Gamma^k N \mathbf{1}\right), \tag{20}$$

where $\boldsymbol{\gamma}^k = [\gamma_i^k, \ldots, \gamma_n^k]^\top$. Computing $N^{-1}W^k\Gamma^k N\mathbf{1}$ yields

$$N^{-1}W^k\Gamma^k N\mathbf{1} = N^{-1}\begin{bmatrix} \sum_{j\neq 1} \gamma_j^k w_{1j}^k N_j \\ \vdots \\ \sum_{j\neq n} \gamma_j^k w_{nj}^k N_j \end{bmatrix}. \tag{21}$$

Using (10), we can write (21) as

$$N^{-1}\begin{bmatrix} \sum_{j\neq 1} F_{1j}^k \\ \vdots \\ \sum_{j\neq n} F_{nj}^k \end{bmatrix} = \begin{bmatrix} \sum_{j\neq 1} \frac{F_{1j}^k}{N_1} \\ \vdots \\ \sum_{j\neq n} \frac{F_{nj}^k}{N_n} \end{bmatrix}, \tag{22}$$

which, by Assumption 1 and (7), becomes

$$\begin{bmatrix} \sum_{i\neq 1} \frac{F_{i1}^k}{N_1} \\ \vdots \\ \sum_{i\neq n} \frac{F_{in}^k}{N_n} \end{bmatrix} = \begin{bmatrix} \gamma_1^k \\ \vdots \\ \gamma_n^k \end{bmatrix} = \boldsymbol{\gamma}^k.$$

Thus, $L^k \mathbf{1} = \mathbf{1}$, showing that L^k meets the requirements to guarantee consensus of the susceptible states as stated in Lemma 2. Therefore, $s_i^* = \alpha$ for all $i \in [n]$, where by Lemma 1 we have that $\alpha \in [0,1]$. $\qquad\square$

IV. FEEDBACK CONTROL

We now propose a feedback control strategy for the model in (13) derived from the current infection states. Given that γ_i^k represents the unimpeded flow out of sub-population i at time step $k \in \mathbb{Z}_{\geq 0}$, we can implement a scheme that restricts travel between all sub-populations proportionally:

$$\tilde{\gamma}_i^k = \theta^k \gamma_i^k, \tag{23}$$

where $\theta^k \in [0,1]$ is the flow restriction penalty. We propose a flow restriction penalty that is a function of the average infection level:

$$\theta^k = 1 - (\bar{x}^k)^{\frac{1}{\eta}}, \tag{24}$$

where $\bar{x}^k = \frac{1}{n}\sum_{i\in[n]} x_i^k$ is the average proportion of infected individuals across all sub-populations and $\eta \in \mathbb{R}_{>0}$ can be viewed as a sensitivity parameter, where $\eta > 1$ denotes a higher sensitivity and $\eta < 1$ denotes a lower sensitivity to the average infection level in the network. The magnitude of η can also be viewed as the strength of the controller in reaction to the overall infection. We now show that applying the strategy in (23) still maintains the assumptions imposed in Section

II, enforcing that the model remains well defined. We define $\widetilde{(13)}$ as the system with dynamics in (13) including the control strategy in (23).

Proposition 1. *Consider* $\widetilde{(13)}$ *under Assumption 2 and with* $\theta^k \in [0,1]$ *for all* $k \geq 0$. *If with* $s_i^0, e_i^0, x_i^0, r_i^0 \in [0,1]$ *and* $s_i^0 + e_i^0 + x_i^0 + r_i^0 = 1$ *for all* $i \in [n]$, *then* $s_i^k, e_i^k, x_i^k, r_i^k \in [0,1]$ *and* $s_i^k + e_i^k + x_i^k + r_i^k = 1$, *for all* $k \geq 0$ *and* $i \in [n]$.

Proof. As control is only applied to γ_i^k for all $i \in [n]$, we must only verify that Assumption 1 is met under the proposed control strategy and the rest will follow from Lemma 1. Since $\theta^k \in [0,1]$ we have by (7) that $\tilde{\gamma}_i^k \in [0,1]$. Furthermore, by (10) we have

$$\tilde{F}_{ij}^k = \tilde{\gamma}_j^{\,k} w_{ij}^k N_j. \tag{25}$$

Computing the flows in versus the flows out, $\tilde{F}^+ - \tilde{F}^-$, yields

$$
\begin{aligned}
\tilde{F}^+ - \tilde{F}^- &= \sum_{j \neq i} \tilde{F}_{ij}^k - \sum_{j \neq i} \tilde{F}_{ji}^k \\
&= \sum_{j \neq i} \tilde{\gamma}_j^{\,k} w_{ij}^k N_j - \sum_{j \neq i} \tilde{\gamma}_i^{\,k} w_{ji}^k N_i \\
&= \theta^k \left(\sum_{j \neq i} \gamma_j^k w_{ij}^k N_j - \sum_{j \neq i} \gamma_i^k w_{ji}^k N_i \right) \\
&= \theta^k (F^+ - F^-) = 0.
\end{aligned}
$$

Thus, Assumption 1 is maintained. Therefore, by Lemma 1 $s_i^k, e_i^k, x_i^k, r_i^k \in [0,1]$ and $s_i^k + e_i^k + x_i^k + r_i^k = 1$, for all $k \geq 0$ and $i \in [n]$. $\qquad\square$

By restricting γ_i^k, we directly reduce the flow of both infected and non-infected individuals according to (9) as

$$\theta^k \left(p_i^{T,k}(s_i^k + e_i^k + r_i^k) + p_i^{x,k} x_i^k \right) = \theta^k \gamma_i^k. \tag{26}$$

Thus, our controlled flow rates, with respect to the conditional probability parameters, are given by

$$\tilde{p}_i^{q,k} = \theta^k p_i^{q,k} \tag{27}$$

where $p_i^{q,k} \in \{p_i^{s,k}, p_i^{e,k}, p_i^{x,k}, p_i^{r,k}\}$.

The control strategy in (23)-(24) effectively restricts flow between all sub-populations proportionally in the presence of any amount of system infection. Note that by construction $\theta^k = 1 - (\bar{x}^k)^{\frac{1}{\eta}} \in [0,1]$ for all $k \geq 0$. Thus, by Proposition 1, the system is well defined.

It should be noted that while proportional restrictions to all flow are not the most precise form of control that can be applied to this model, this approach is not dissimilar to the travel policies on global and regional flights during the height of the COVID-19 pandemic [19]. In the following section we apply this control strategy to a simplified model of a travel network between populous cities based on median flight data, and evaluate its effectiveness on mitigating disease spread.

V. SIMULATIONS

In this section, we detail the methods and parameters used to simulate our model, its limiting behavior, and our proposed control strategy as described in Sections II-IV. We construct our simulations using population data from the US cities of Atlanta, Los Angeles, Chicago, and Dallas, and the flights between each city's primary airport (ATL, LAX, ORD, DFW).
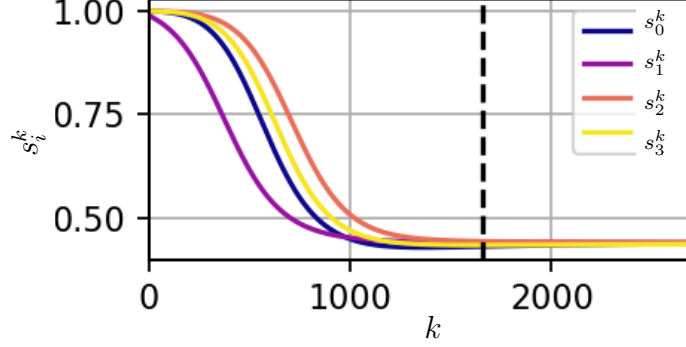
FIGURE 1: An illustration of the model in (13) reaching consensus after the infection dies out in the system, indicated by the vertical black dotted line where $\bar{x} \leq 10^{-4}$.

The infection starts in Los Angeles and propagates through the network, reaching an equilibrium where $x_i^k = 0$ for all $i \in [n]$.

To simulate the states for the SEIR model we use (13) with fixed homogeneous spread parameters (i.e., the same for every sub-population and static), $(\beta, \delta, \sigma, h, p^x) = (0.5, 0.34, 0.19, 0.14, 0.005)$. The population of each city is given by $(N_{\text{ATL}}, N_{\text{LAX}}, N_{\text{ORD}}, N_{\text{DFW}}) \approx (0.5, 4, 2.7, 1.3) * 10^6$, where the population sizes are approximated from [20] and [21]. The population traveling between the cities is approximated by the median number of daily flights between the airports in March 2021 [22]:

$$F = \xi \begin{bmatrix} 0 & 15 & 23 & 19 \\ 15 & 0 & 22 & 21 \\ 23 & 22 & 0 & 23 \\ 19 & 21 & 23 & 0 \end{bmatrix},$$

where $\xi \in \mathbb{R}_{\geq 0}$ is a scaling factor, which is used to increase or decrease the total volume of population flow. The initial conditions for the sub-populations are $s^0 = [1, 0.99, 1, 1]$, $e^0 = [0, 0.005, 0, 0]$, $x^0 = [0, 0.005, 0, 0]$, and $r^0 = [0, 0, 0, 0]$.

First, we show the consensus behavior from Theorem 1 by simulating (13) using the given initial conditions and model parameters. In Figure 1, we see that the susceptible proportions of sub-populations reach consensus. The dashed vertical line in the graph indicates the time step at which the average infected proportion of the population reaches near zero ($\bar{x}^k \leq 10^{-4}$). These results suggest that, by the end of the epidemic process, the flow dynamics dominate the behavior of the model and eventually lead to an equal mixing of susceptible and recovered populations given enough time, as suggested by Theorem 1.

Second, we simulate the control strategy proposed in Section IV with and without an additional heuristic for vaccine distribution. With no vaccine strategy applied, these simulations show that exclusively implementing a control law that uniformly reduces travel based on $\bar{x}^k$, namely using (23)-(24), does not have a significant impact on the total number of people infected. Furthermore, in many cases increasing the strength of the controller will cause the total number of recovered individuals to increase. This phenomenon is illustrated in the plot at the bottom of Figure 2 by the fact that as the x-axis increases (recall that the η value corresponds to the strength of the controller), so does $\bar{r}^*$ (except for very small γ values). This behavior is the consequence of at least two reasons: 1) the controller does not prevent infections from occurring inside the sub-populations (i.e. no lock downs), and 2) the controller in some cases 'flattens the curve' which prolongs the outbreak
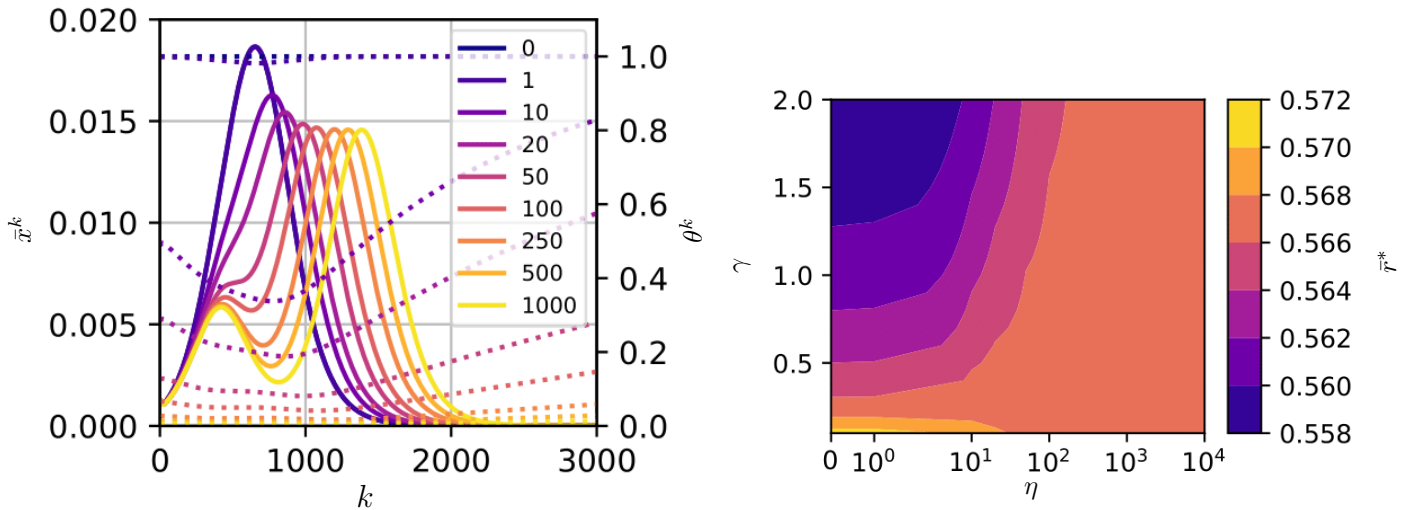
FIGURE 2: System response to the controller in (23)-(24) with different strength values (η) and flow rates (γ). (Top) Plot of $\bar{x}^k$ with η ranging from 0 to 1000 and $\xi = 100$. An $\eta = 0$ means the control strategy is not used. The dotted lines of corresponding color denote the control penalty applied to the flow rates in the system with respect to the total infection level. (Bottom) The average proportion of recovered individuals $\bar{r}^*$ for a spectrum of equilibria. The baseline $\gamma = 1.0$ is when $\xi = 100$.
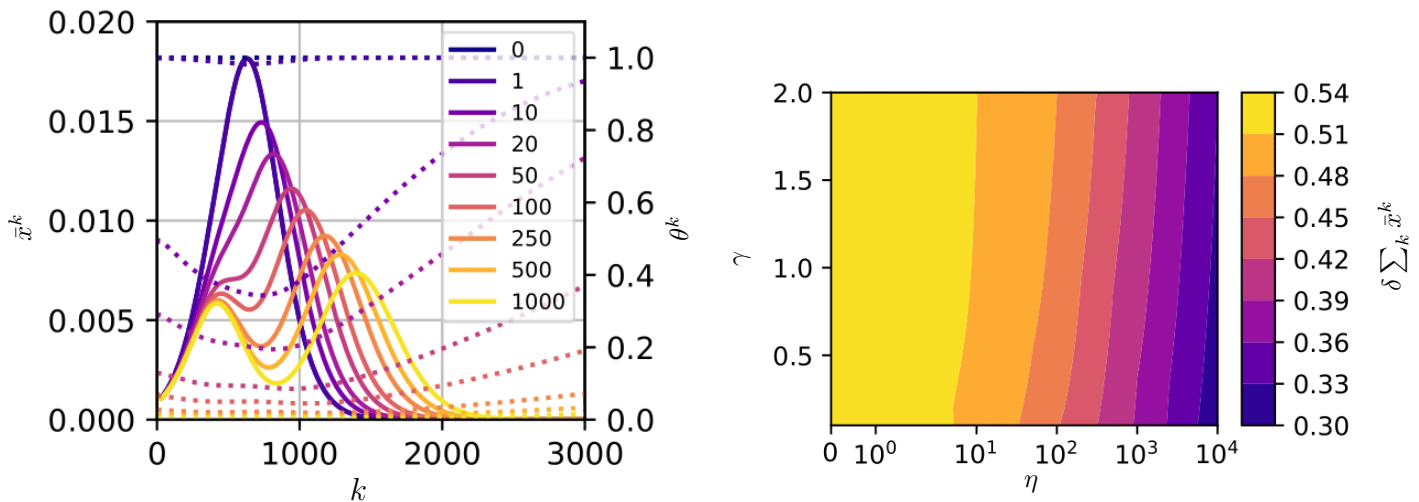

FIGURE 3: Implementation of a vaccine roll-out. Plots mirror those in Figure 2, with the roll-out starting at $k = 500$, moving 0.1% of $s_i^k \to r_i^k$ until $\bar{s}^k = 0.01$. (Top) Plot of $\bar{x}^k$ with η ranging from 0 to 1000 and $\xi = 100$. An $\eta = 0$ means the control strategy is not used. The dotted lines of corresponding color denote the control penalty applied to the flow rates in the system with respect to the total infection level. (Bottom) The average proportion of recovered individuals due to infection $\delta \sum_k \bar{x}^k$, which is equivalent to $\bar{r}^*$ when there is no vaccine, for a spectrum of equilibria. The baseline $\gamma = 1.0$ is when $\xi = 100$.
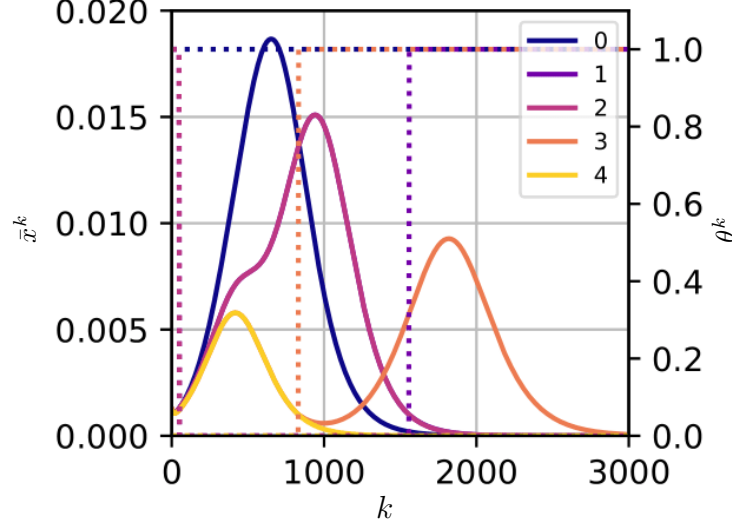
FIGURE 4: System response (solid lines) to the controller in (23) with an on-off flow penalty (dotted lines). The case $\eta = 0$ has $\theta^k = 1$ for all $k \geq 0$, the cases $\eta = 1, 2$ have $\theta^k = 1$ for all $k \in \{0, \ldots, 49\}$ and set $\theta^k = 0$ starting at $k = 50$, the cases $\eta = 3, 4$ have $\theta^k = 0$ starting from $k = 0$, cases $\eta = 1, 3$ re-open travel (set $\theta^k = 1$) for all k after $\bar{x}^k < 0.001$, and cases $\eta = 2, 4$ only re-open travel after $\bar{x}^k \approx 0$.

and increases the integral under the curve (i.e. a higher number of total infections).

On the other hand, a reduction in the peak infected population reduces strain on healthcare systems, improving medical outcomes and decreasing fatality rates [23], and creates an opportunity for a vaccine to be more impactful. In Figure 3 we simulate the network with the same initial conditions and parameters as Figure 2, adding the distribution of a vaccine, starting at time step $k = 500$, which, for each sub-population, moves 0.1% percent of the susceptible proportion directly to the recovered proportion at each time step. In the bottom of Figure 3, we show the mean infected proportion of the system for increasing levels of sensitivity as well as the total proportion of the recovered population who were infected by the disease ($\delta \sum_{k \geq 0} \bar{x}^k$). We see that a combined strategy of restricting flow and vaccine distribution can have a marked effect on the number of individuals infected while simultaneously reducing the peak infection level of the system.

Lastly, we implement the controller in (23) with θ^k being strictly binary, that is, θ^k is either 0 or 1. In Figure 4, control strategies $\eta = 1, 2$ shut down all travel after 50 time steps, imitating a delay in decision making from policymakers while strategies $\eta = 3, 4$ shut down travel immediately when the infection is first detected in any sub-population. A critical note is that even when travel is eventually completely closed, if it does not happen quickly enough then there will be almost no discernible impact on infection levels, as seen by comparing control strategies $\eta = 1, 2$. These extreme cases illustrate that unless the infection is completely eradicated ($\bar{x}^k = 0$) prior to reopening travel, it will always spread throughout the network after travel is reopened. When we tested the binary controller case $\eta = 3$ reopening travel after $\bar{x}^k < 10^{-9}$, there was a second $\bar{x}^k$ peak around $k = 7000$. When a vaccine is distributed, this delayed second wave can be significantly mitigated as shown in Figure 5. While costly, completely closing all travel between sub-populations can enable a vaccine to have a tremendous impact but only if the initial response is not delayed.
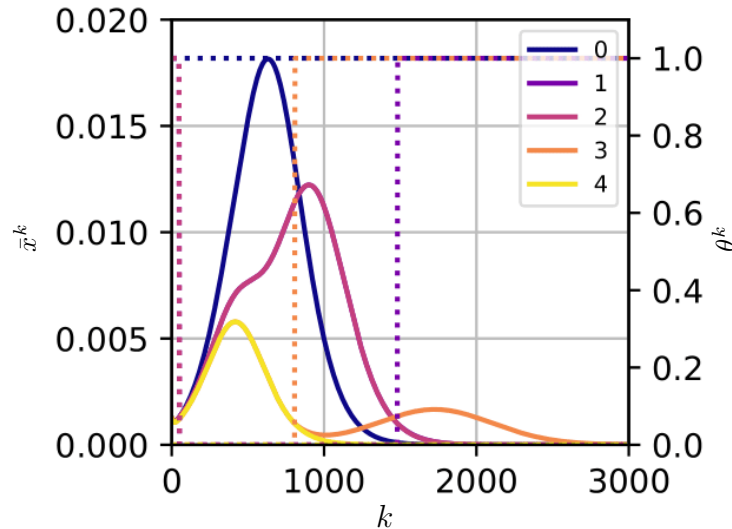
FIGURE 5: System response to the controller in (23) with an on-off flow penalty combined with a vaccine roll-out. The on-off controller is identical to Figure 4 and the vaccine roll-out is identical Figure 3.

VI. Conclusion

In this paper, we have constructed a networked discrete-time SEIR epidemic model that incorporates population flows, presented conditions under which the model is well-defined, and shown asymptotic convergence to the healthy states, the set of equilibria. Additionally, we have proposed a control policy for restricting population flow which can be interpreted as implementing travel restrictions/bans, showed it is well defined, and illustrated its behavior via simulation. We have found that only restricting the flow of the population is typically insufficient to reduce the total number of infections over the course of an epidemic. More severe restrictions on the population flow can decrease the peak infection level, which can alleviate stress on healthcare facilities. Further, applying population flow restrictions together with a vaccination strategy can significantly reduce the total number of infections.

For future work we plan to incorporate the possibility of infections occurring while individuals are traveling (i.e., infections occurring on the edges of the graph) as well as using real travel and infection data from the COVID-19 pandemic to learn the model parameters. Finally, note that our model does not capture asymptomatic transmission of the virus, a key component of the infectious behavior of COVID-19, therefore, developing a similar SAIR formulation remains open to future work.

References

[1] S. Ruan, W. Wang, and S. A. Levin, "The effect of global travel on the spread of SARS," *Mathematical Biosciences & Engineering*, vol. 3, no. 1, p. 205, 2006.

[2] A. J. Tatem, D. J. Rogers, and S. I. Hay, "Global transport networks and infectious disease spread," *Advances in Parasitology*, vol. 62, pp. 293–343, 2006.

[3] A. J. Rodríguez-Morales, K. MacGregor, S. Kanagarajah, D. Patel, and P. Schlagenhauf, "Going global–travel and the 2019 novel coronavirus," *Travel Medicine and Infectious Disease*, vol. 33, p. 101578, 2020.

[4] K. Rock, S. Brand, J. Moir, and M. J. Keeling, "Dynamics of infectious diseases," *Reports on Progress in Physics*, vol. 77, no. 2, p. 026602, 2014.

[5] W. Mei, S. Mohagheghi, S. Zampieri, and F. Bullo, "On the dynamics of deterministic epidemic propagation over networks," *Annual Reviews in Control*, vol. 44, pp. 116–128, 2017.

[6] J. A. Backer, D. Klinkenberg, and J. Wallinga, "Incubation period of 2019 novel coronavirus (2019-nCoV) infections among travellers from Wuhan, China, 20–28 January 2020," *Eurosurveillance*, vol. 25, no. 5, p. 2000062, 2020.

[7] W. Guan, Z. Ni, Y. Hu, W. Liang, C. Ou, J. He, L. Liu, H. Shan, C. Lei, D. S. Hui *et al.*, "Clinical Characteristics of Coronavirus Disease 2019 in China," *New England Journal of Medicine*, vol. 382, no. 18, pp. 1708–1720, 2020.

[8] Q. Li, X. Guan, P. Wu, X. Wang, L. Zhou, Y. Tong, R. Ren, K. S. Leung, E. H. Lau, J. Y. Wong *et al.*, "Early transmission dynamics in Wuhan, China, of novel coronavirus–infected pneumonia," *New England Journal of Medicine*, 2020.

[9] S. A. Lauer, K. H. Grantz, Q. Bi, F. K. Jones, Q. Zheng, H. R. Meredith, A. S. Azman, N. G. Reich, and J. Lessler, "The incubation period of coronavirus disease 2019 (COVID-19) from publicly reported confirmed cases: Estimation and application," *Annals of Internal Medicine*, vol. 172, no. 9, pp. 577–582, 2020.

[10] O. Byambasuren, M. Cardona, K. Bell, J. Clark, M.-L. McLaws, and P. Glasziou, "Estimating the extent of true asymptomatic COVID-19 and its potential for community transmission: Systematic review and meta-analysis," *Official Journal of the Association of Medical Microbiology and Infectious Disease Canada*, vol. 5, no. 4, pp. 223–234, 2020.

[11] D. Chang, G. Mo, X. Yuan, Y. Tao, X. Peng, F.-S. Wang, L. Xie, L. Sharma, C. S. Dela Cruz, and E. Qin, "Time kinetics of viral clearance and resolution of symptoms in novel coronavirus infection," *American Journal of Respiratory and Critical Care Medicine*, vol. 201, no. 9, pp. 1150–1152, 2020.

[12] K. Mizumoto, K. Kagaya, A. Zarebski, and G. Chowell, "Estimating the asymptomatic proportion of coronavirus disease 2019 (COVID-19) cases on board the Diamond Princess cruise ship, Yokohama, Japan, 2020," *Eurosurveillance*, vol. 25, no. 10, p. 2000180, 2020.

[13] A. J. Ing, C. Cocks, and J. P. Green, "COVID-19: In the footsteps of Ernest Shackleton," *Thorax*, 2020.

[14] M. Ye, J. Liu, C. Cenedese, Z. Sun, and M. Cao, "A network SIS meta-population model with transportation flow," in *Proceedings of the IFAC World Congress*, 2020.

[15] D. Brockmann and D. Helbing, "The hidden geometry of complex, network-driven contagion phenomena," *Science*, vol. 342, no. 6164, pp. 1337–1342, 2013.

[16] D. Vrabac, M. Shang, B. Butler, J. Pham, R. Stern, and P. E. Paré, "Capturing the effects of transportation on the spread of COVID-19 with a multi-networked SEIR model," *IEEE Control Systems Letters*, 2021.

[17] H. Shu, D. Fan, and J. Wei, "Global stability of multi-group SEIR epidemic models with distributed delays and nonlinear transmission," *Nonlinear Analysis: Real World Applications*, vol. 13, no. 4, pp. 1581–1592, 2012.

[18] V. D. Blondel, J. M. Hendrickx, A. Olshevsky, and J. N. Tsitsiklis, "Convergence in multiagent coordination, consensus, and flocking," in *Proceedings of the 44th IEEE Conference on Decision and Control*.   IEEE, 2005, pp. 2996–3000.

[19] T. Suzumura, H. Kanezashi, M. Dholakia, E. Ishii, S. A. Napagao, R. Pérez-Arnal, and D. Garcia-Gasulla, "The impact of COVID-19 on flight networks," *arXiv preprint arXiv:2006.02950*, 2020.

[20] "Annual estimates of the resident population for incorporated places of 50,000 or more," 2019. [Online]. Available: https://www.census.gov/data/tables/time-series/demo/popest/2010s-total-cities-and-towns.html

[21] "Place explorer." [Online]. Available: https://datacommons.org/place

[22] "All routes and scheduled flights from every airport." [Online]. Available: https://www.flightsfrom.com/

[23] C. Kenyon, "Flattening-the-curve associated with reduced COVID-19 case fatality rates-an ecological analysis of 65 countries," *Journal of Infection*, vol. 81, no. 1, pp. e98–e99, 2020.